RESEARCH ARTICLE
SPACE PHYSICS

Earth and Planetary Physics
10: 117–125, 2026
doi: 10.26464/epp2026004

First systematic identification of triple-mode Auroral Kilometric Radiation using Arase polarization data

YiHua He[1*], SanGuang Li[1], HongMing Yang[2], Sai Zhang[1*], YuYue Jin[1], Si Liu[1], ZhongLei Gao[1], FuLiang Xiao[1*], ZhaoGuo He[3], JiaWen Tang[1], and Ping Li[1]

[1]School of Physics and Electronic Sciences, Changsha University of Science and Technology, Changsha 410114, China;

[2]School of Electrical and Information Engineering, Changsha University of Science and Technology, Changsha 410114, China;

[3]State Key Laboratory of Lunar and Planetary Sciences, Macau University of Science and Technology, Macao 999078, China

Key Points:

- A practical method for calculating wave polarization using the Arase satellite data
- By combining polarization and frequency analysis, the wave mode of AKR (Auroral kilometric radiation) is identified.
- It is demonstrated that AKR in R-X, L-O, and L-X modes can be observed on both the dayside and nightside.

Citation: He, Y. H., Li, S. G., Yang, H. M., Zhang, S., Jin, Y. Y., Liu, S., Gao, Z. L., Xiao, F. L., He, Z. G., … Li, P. (2026). First systematic identification of triple-mode Auroral Kilometric Radiation using Arase polarization data. *Earth Planet. Phys.*, *10*(1), 117–125. http://doi.org/10.26464/epp2026004

Abstract: Auroral kilometric radiation (AKR), a fundamental plasma emission in Earth's magnetosphere, exhibits three characteristic modes: the right-handed extraordinary (R-X), left-handed ordinary (L-O) and left-handed extraordinary (L-X) modes. The role of AKR in magnetosphere–ionosphere–atmosphere coupling depends sensitively on its wave mode. While previous studies have primarily focused on the dominant R-X mode, we present the first systematic identification of all three modes using a practical polarization analysis method based on Arase satellite observations. This method employs a spin-axis-relative Ratio: when the satellite's spin axis aligns with the background magnetic field, a positive (negative) *Ratio* indicates the right-handed (left-handed) polarization, with reversal under anti-parallel conditions. Combined polarization-frequency analysis reveals that R-X, L-O, and L-X modes can exist in both dayside and nightside regions, with power spectral densities up to 10^{-6} $mV^2m^{-2}Hz^{-1}$. This study resolves long-standing ambiguities in AKR mode classification and has implications for understanding AKR-induced electron dynamics.

Keywords: Auroral kilometric radiation; wave mode; polarization

1. Introduction

Auroral kilometric radiation (AKR), a powerful terrestrial radio emission originating in polar, magnetic field-aligned cavities, is fundamentally linked to magnetosphere–ionosphere–atmosphere coupling (Kurth et al., 1975; Ergun et al., 1998; Zarka, 1998; Mutel et al., 2008; Xiao FL et al., 2010). The generation mechanism of AKR most widely accepted is the electron cyclotron maser instability (ECMI) (Wu CS and Lee, 1979; Melrose et al., 1982; Pritchett, 1984; Calvert, 1995; Mutel et al., 2007; Burinskaya, 2013). The generation of AKR necessitates downward superthermal electrons to provide free energy (Delory et al., 1998; Ergun et al., 1998; Seki et al., 2005; Jiao LH et al., 2024; Jin TF et al., 2025). A positive velocity gradient in the electron velocity distribution leads to a significant nonlinear growth of the wave near the electron cyclotron frequency, which is usually necessary in the simulations of AKR generation (Mutel et al., 2007). Previous studies have shown that AKR exhibits significant correlations with magnetospheric activity in terms of both intensity and frequency characteristics (Kurth and Gumett, 1998; Liou et al., 2000), while also demonstrating distinct seasonal variations (Kumamoto et al., 2003). Li P et al. (2024) have shown that the occurrence of AKR is related to interplanetary magnetic field and has obvious seasonal characteristics. Tang JW et al. (2025) have found that there is an obvious spatial asymmetry in the distribution of AKR. Numerous studies have demonstrated that AKR can effectively accelerate or scatter energetic electrons under the appropriate conditions (Summers et al., 2001; Xiao FL et al., 2006; Zhang S et al., 2020). Those electrons have serious damage to the ozone layer and spacecraft (Thorne, 1977; Callis et al., 1998; Baker, 2002; Thorne et al., 2005). Zhao WL et al. (2019) have found that AKR is widely distributed in the region of L = 3–6.5 and MLT = 00–24 using the observations from Van Allen probes. Zhang S et al. (2021) have presented a simplified model of the field-aligned distribution of AKR mode amplitude in the region of L = 3.0–6.2 and Mlat = 0°–±40° using the observations from the Arase satellite and Van Allen Probes. Through the work of other researchers, it is now possible to determine the annual and seasonal periodic variations of AKR mode (Kumamoto et al., 2003; Green et al., 2004; Mogilevsky et al., 2005; Xiao FL et al., 2022).

Correspondence to: S. Zhang, saizh@126.com
F. L. Xiao, flxiao@126.com
Y. H. He, heyihua16@sina.com

Received 17 JUN 2025; Accepted 28 AUG 2025.
First Published online 09 SEP 2025.

According to the dispersion relation of plasma waves, AKR has three modes, named the right-handed extraordinary (R-X), left-handed ordinary (L-O) and left-handed extraordinary (L-X) modes (Sonwalkar et al., 2004). Previous studies have demonstrated that AKR mainly occurs in the R-X mode, with less occurrence in the L-O and L-X modes (Calvert, 1981a, b; Gurnett et al., 1983; Liou et al., 2000; Pritchett et al., 2002; Schreiber et al., 2017). Critically, the role of AKR in these coupling processes exhibits strong mode dependence (Xiao FL et al., 2011). Despite this modal diversity, our understanding remains incomplete. Xiao FL et al. (2016) have demonstrated that R-X mode can propagate downward to the equatorial plane from high latitudes using 3-D ray tracing, and Deng ZK et al. (2022) have provided a direct observational evidence. Extensive statistical studies and case analyses have established the R-X mode as the primary emission, revealed its global distribution across L-shells, magnetic latitude (Mlat), and magnetic local time (MLT). Observations of L-O mode are fewer, showing complexities: while often appearing weaker and at lower frequencies than R-X in simultaneous detections (Kumamoto et al., 2018). Hanasz et al. (2003) have performed a statistical study of the occurrence distributions of R-X and L-O modes and analyzed the source region of AKR. Observations have found that L-O mode appears at lower frequency range and is much weaker than R-X mode when the R-X and L-O modes were present simultaneously (Shawhan and Gurnett, 1982; Mellott et al., 1984; Benson et al., 1988). Instances of strong or even dominant L-O emissions were also reported, attributed to refraction and reflection the of R-X mode near sharp density gradients (plasmapause) (Kaiser et al., 1978; Oya and Morioka, 1983; Benson, 1985; Hanasz et al., 2000). This is due to the refraction and reflection of the R-X mode by the density gradient near the source region and the plasmapause. However, direct observational evidence for the L-X mode emission remains scarce (Zhang S et al., 2024).

Since comprehensive analyses encompassing all three AKR modes have been lacking, limiting our ability to quantify their mode-specific contributions to electron dynamics, we adopt a practical polarization analysis technique applied to high-resolution wave observations from the Arase satellite to directly identify all three modes.

2. Method of Polarization Analysis

AKR is the superluminous waves in the magnetosphere with wave phase speed greater than the speed of light (Xiao FL et al., 2010). The general dispersion relation for the superluminous wave in collisionless, cold plasma, with negligence of ion motion, has been formulated (Xiao FL et al., 2006):

$$\mu^2 = \mu_{\mp}^2 = 1 - \frac{f_{pe}^2}{f^2}\Psi_{\mp}^{-1}, \tag{1}$$

$$\Psi_{\mp} = 1 - \frac{f_{ce}^2\sin^2\theta}{2(f^2 - f_{pe}^2)} \mp \left[\left(\frac{f_{ce}^2\sin^2\theta}{2(f^2 - f_{pe}^2)}\right)^2 + \frac{f_{ce}^2\cos^2\theta}{f^2}\right]^{1/2}, \tag{2}$$

where μ is the refractive index of plasma waves, f is the wave frequency, f_{pe} is the plasma angular frequency and f_{ce} is the electron gyro-frequency, θ is the wave normal angle. The dispersion relations and frequency ranges of three modes are given as follows:

$$\text{R-X} \quad \text{mode}: \mu = \mu_{-}, f > f_{RX}, \tag{3}$$

$$\text{L-O} \quad \text{mode}: \mu = \mu_{+}, f > f_{pe}, \tag{4}$$

$$\text{L-X} \quad \text{mode}: \mu = \mu_{+}, f_{LX} < f < f_{pe}, \tag{5}$$

with

$$f_{RX} = [f_{ce} + (f_{ce}^2 + 4f_{pe}^2)^{1/2}]/2, \tag{6}$$

$$f_{LX} = [-f_{ce} + (f_{ce}^2 + 4f_{pe}^2)^{1/2}]/2. \tag{7}$$

In order to judge the modes of AKR, we should identify the polarization of plasma wave. It is well known that the characteristics of wave modes in any direction of propagation can be understood as a transition between two special cases: propagation parallel or perpendicular to the external magnetic field. When the direction of the wave propagation is parallel to the magnetic field direction, for the right-hand polarized wave, the ratio of the two electric field components in the plane perpendicular to the wave vector is

$$E_x/E_y = e^{i(-\pi/2)} = -i.$$

For the left-hand polarized wave, the corresponding ratio is

$$E_x/E_y = e^{i(\pi/2)} = i.$$

However, it is difficult to directly measure the two electric field components perpendicular to the magnetic field. Therefore, to accurately determine the polarization state of waves, it is essential to obtain the Stokes parameters (I, Q, U, V). This can be achieved using a spacecraft equipped with a triaxial orthogonal antenna system. The polarization of the wave is then determined based on the sign of the Stokes parameter V, the relative position between the satellite and the wave source, and the direction of the ambient magnetic field. The specific methodology is analogous to that employed by the Arase satellite and will not be elaborated upon here. I is power density of the emission, Q and U are linear polarization parameters normalized to I, and V circular polarization parameters normalized to I (relative to the spacecraft spin axis). The Stokes parameters I, Q, U, and V are derived from outputs of the four channels S_y, S_z, S_{y+z}, and S_{y+iz} using the following formula (Hanasz et al., 2000, 2003; Panchenko, 2004):

$$I = S_y + S_z, \tag{8}$$

$$Q = \frac{S_y - S_z}{I}, \tag{9}$$

$$U = \frac{S_{y+z} - S_y - S_z}{I}, \tag{10}$$

$$V = \frac{S_{y+iz} - S_y - S_z}{I}. \tag{11}$$

Arase satellite was launched by the Japan Aerospace Exploration Agency and began taking measurements on March 2017. The orbit of the Arase is highly elliptical, and the orbital inclination is ~31°. Its altitudes perigee and apogee are 340–440 km and 32, 200–32, 300 km, respectively. The orbit of Arase covers the region of Mlat = 0–±42°. When the satellite is located the high magnetic latitude, the satellite can reach the region of L = 10–11 (Miyoshi et al., 2018; Nakamura et al., 2018). The Wire Probe Antenna (WPT) onboard the Arase comprises two pairs of dipole antennas with a length of ~31 meters from tip to tip. The two pairs of antennas are orthogonal to each other and perpendicular to the spin axis of Arase (Kasaba et al., 2017). The High Frequency Analyzer (HFA) of the Plasma Wave Experiment (PWE) on the Arase spacecraft can measure the power spectral density (PSD) of the wave electric

field. The analyzer can measure the electric field component of the plasma wave in the frequency range of 2 kHz to 10 MHz (Kasahara et al., 2018; Kumamoto et al., 2018).

The Arase satellite uses a simplified method to determine the polarization of waves. The Arase satellite can detect two electric field components, E_u and E_v, using WPT sensors (WPT-S-U1, WPT-S-U2, WPT-S-V1, and WPT-S-V2). After E_u and E_v are converted into voltage signals, they are fed into the HFA through the amplifier. The HFA is capable of obtaining the electric field power spectrum, as well as the left-hand (E_L) and right-hand (E_R) electric fields through specific processing and analysis methods. E_L and E_R are calculated as follows:

$$E_L^2 = \frac{\tilde{E}_u^2 + \tilde{E}_v^2}{2} - \mathrm{Im}\tilde{E}_u\tilde{E}_v^*, \tag{12}$$

$$E_R^2 = \frac{\tilde{E}_u^2 + \tilde{E}_v^2}{2} + \mathrm{Im}\tilde{E}_u\tilde{E}_v^*, \tag{13}$$

where * indicates a complex conjugate and Im indicates an imaginary part. $\tilde{E}_u$ and $\tilde{E}_v$ are the Fourier complex coefficients of E_u and E_v, respectively. Using $\langle E_L^2\rangle$ and $\langle E_R^2\rangle$ ($\langle\rangle$ represents the ensemble average of eight raw spectra obtained during one spin period), the axial *Ratio* of wave can be obtained by the following formula:

$$Ratio = \frac{\langle E_R^2\rangle - \langle E_L^2\rangle}{\langle E_R^2\rangle + \langle E_L^2\rangle}. \tag{14}$$

In order to ensure a sufficient signal-to-noise ratio for reliable polarization determination, we assume that the circular polarization threshold as $|Ratio| = 0.3$. According to the sign of *Ratio*, the polarization relative to the satellite spin axis can be directly determined (ant-sunward direction) (Kumamoto et al., 2018). The polarization of waves is defined with respect to the direction of magnetic field. The direction of magnetic field is sunward (ant-sunward) in the northern hemisphere on the nightside and the southern hemisphere on the dayside (the northern hemisphere on the dayside and the southern hemisphere on the nightside). Therefore, we can obtain the polarization of waves according to the sign of *Ratio* and the space position of the spacecraft. When the satellite is located in the nightside of northern hemisphere or dayside of southern hemisphere, a positive (negative) *Ratio* corresponds to the left-hand (right-hand) polarization. Conversely, when positioned in the dayside of northern hemisphere or nightside of southern hemisphere, a positive (negative) *Ratio* corresponds to right-hand (left-hand) polarization. In this study, we report observations of three modes using the data from the Arase satellite. In general, we focus on strong AKR emissions (PSD $\geq 10^{-8}$

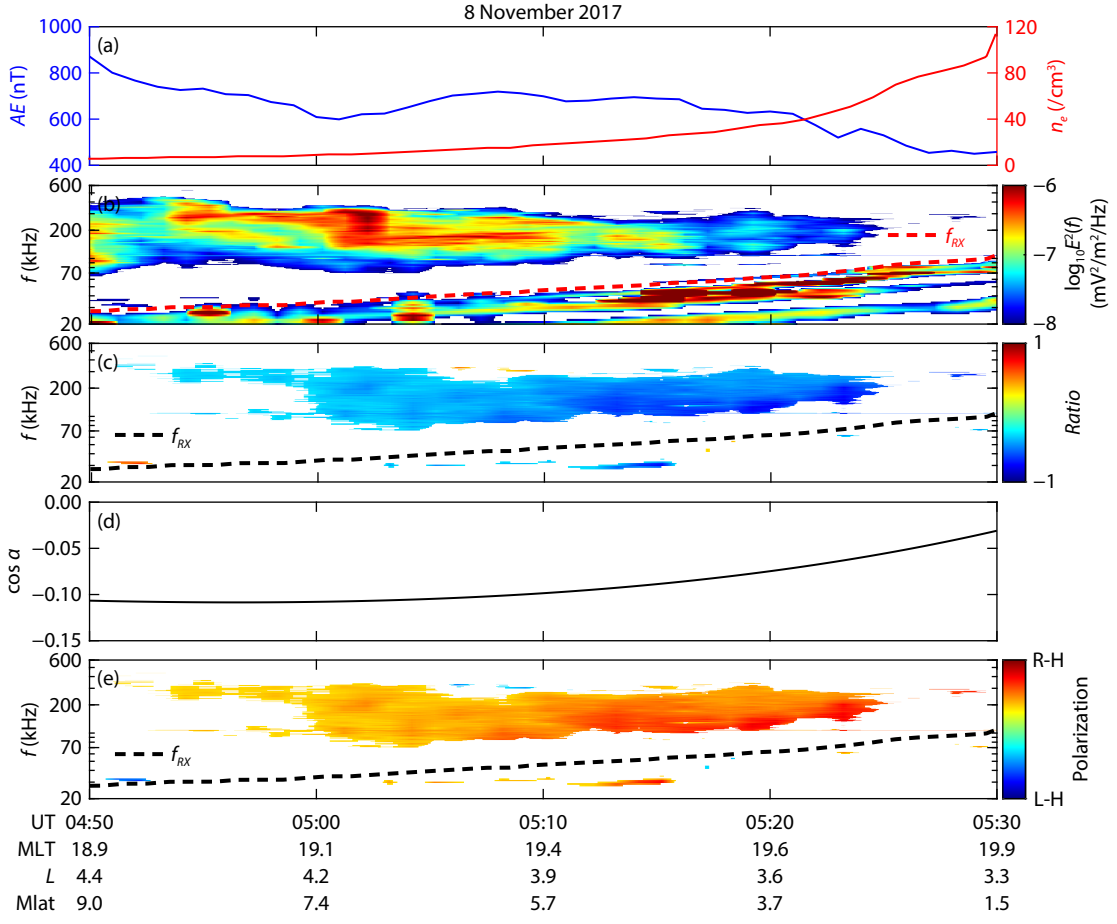

Figure 1. Nightside R-X mode AKR (Event A) observed by the Arase satellite during 04:50–05:30 UT on 8 November 2017. (a) The *AE* index (blue line) and plasma density (red line). (b) The electric field spectra measured by the HFA (the red dashed line represents the f_{RX}). (c) The raw *Ratio* of emissions with PSD $\geq 10^{-8}$ mV^{2}m^{-2}Hz^{-1} (the black dashed line represents the f_{RX}). *Ratio* > 0 (< 0) indicates the left-handed (right-handed) polarization relative to the satellite spin axis. (d) The cosine α (α is defined as the angle between the local background magnetic field and the spin axis). (e) The polarization of emissions with PSD $\geq 10^{-8}$ mV^{2}m^{-2}Hz^{-1} (the black dashed line corresponds to the f_{RX}).

$mV^2m^{-2}Hz^{-1}$) in the magnetosphere.

3. Identification of Three Modes

Using the Arase data, we present six typical AKR events for the three modes as follows. Figure 1 details a strong AKR emission (Event A) recorded on 8 November 2017 (04:50–05:30 UT), occurring on the nightside (MLT = 18.9–19.9, Mlat = 9.0°–1.5°). Figure 1a shows the *AE* index (the blue line) and plasma density (the red line) during the period. The *AE* index could reach ~1000 nT, indicating the relatively strong geomagnetic activity. The plasma density was derived from the upper hybrid resonance frequency, and increased significantly (from 5 to 120 cm^{-3}). As shown in Figure 1b, the HFA detected strong AKR emissions (PSD $\geq$ 10^{-8} $mV^2m^{-2}Hz^{-1}$), with frequencies in the range of 50–600 kHz. The red dashed line represents the cutoff frequency of R-X mode (f_{RX}), and the white area represents PSD <10^{-8} $mV^2m^{-2}Hz^{-1}$. Figure 1c shows the *Ratio* from the Arase satellite data. *Ratio* > 0 (< 0) indicates the left-handed (right-handed) polarization relative to the satellite spin axis. In order to check the direction of background magnetic field, we define α as the angle between the spin axis of satellite and background magnetic field. The cosine α is plotted in Figure 1d. The *Ratio*, verified against the background field direction, indicates the right-handed polarization. Figure 1e shows the polarization clearly maintaining negative values (*Ratio* < −0.3) coincident with significant wave power (PSD $\geq$ 10^{-8} $mV^2m^{-2}Hz^{-1}$) above the f_{RX} (the black dashed line). L-H and R-H indicate the left-handed and right-handed polarization relative to the background magnetic field, respectively. Combined with the high-frequency localization above f_{RX}, it confirms Event A as a dominant R-X mode emission. Contrasting with the active nightside event, Figure 2 presents another R-X mode emission (Event B) observed under relatively quiet geomagnetic conditions (*AE* index was between 50–200 nT) from 04:30 to 05:30 UT on 22 March 2018 on the dayside (MLT = 9.8–10.6). The plasma density (~10 cm^{-3}) remained relatively stable during this period. Clear AKR signatures were detected with PSD about PSD $\geq$ 10^{-8} $mV^2m^{-2}Hz^{-1}$ in the frequency range of 200–500 kHz. Figure 2c shows the *Ratio* from the Arase satellite observation. Figure 2d plots the cosine α. Polarization analysis (Figure 2d) reveals consistently negative *Ratio* values (<−0.3) in the region of enhanced power above f_{RX}, confirming Event B as a dominant R-X mode emission. Figures 1–2 confirm the sustained presence of R-X mode on both dayside and nightside, and the PSD of R-X mode on the nightside can reach 10^{-6} $mV^2m^{-2}Hz^{-1}$.

Figures 3–4 display the examples of L-O mode AKR emissions. As shown in Figure 3, intense AKR emission (Event C) were observed on the nightside (MLT = 1.2–2.4, Mlat = 38.9°–36.2°) during 04:14–04:30 UT on 30 August 2019. The *AE* index (the blue line in Figure 3a) ranged between 40–70 nT, indicating quiet geomagnetic conditions. PSD of the AKR increases to 10^{-6} $mV^2m^{-2}Hz^{-1}$ (Figure 3b), as the plasma density decrease to 450 cm^{-3} (the red line in

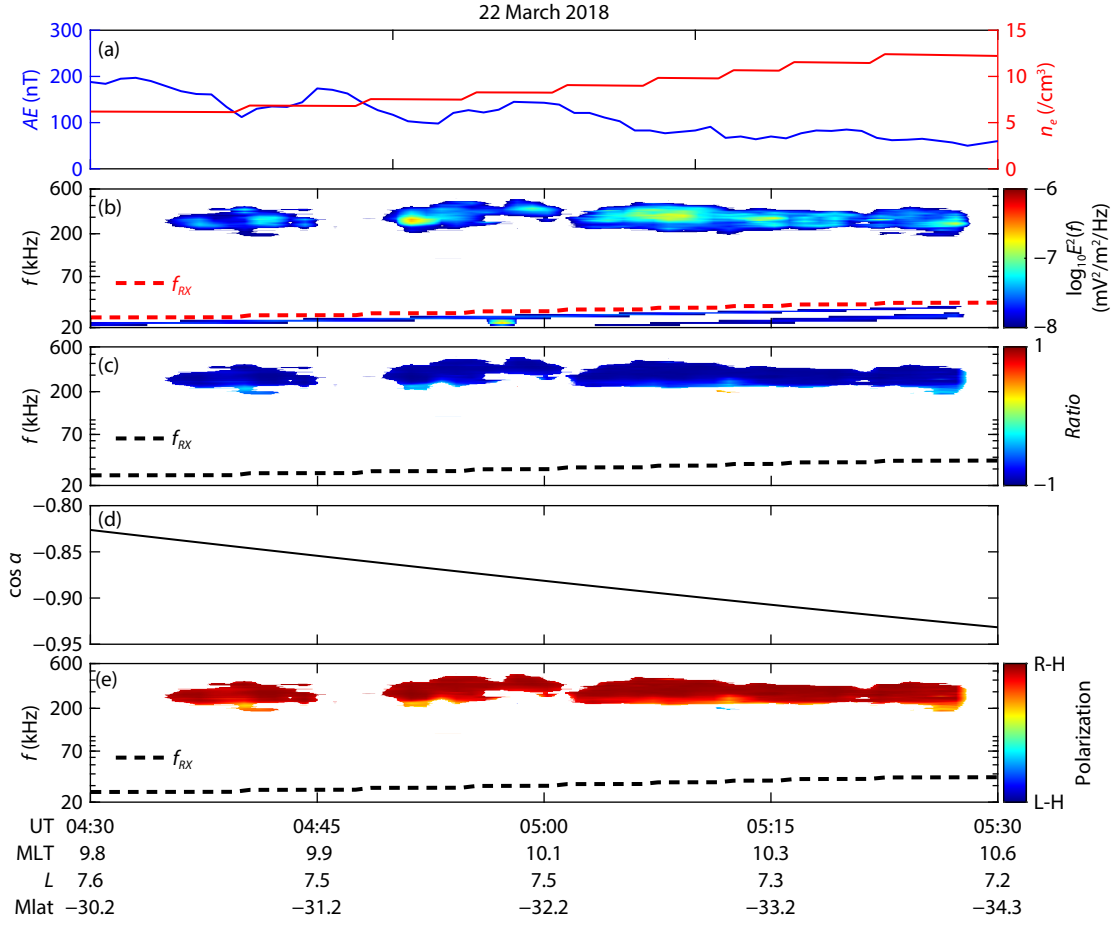

Figure 2. Dayside R-X mode AKR (Event B) observed by the Arase satellite during 04:30–05:30 UT on 22 March 2018. Same format as Figure 1.

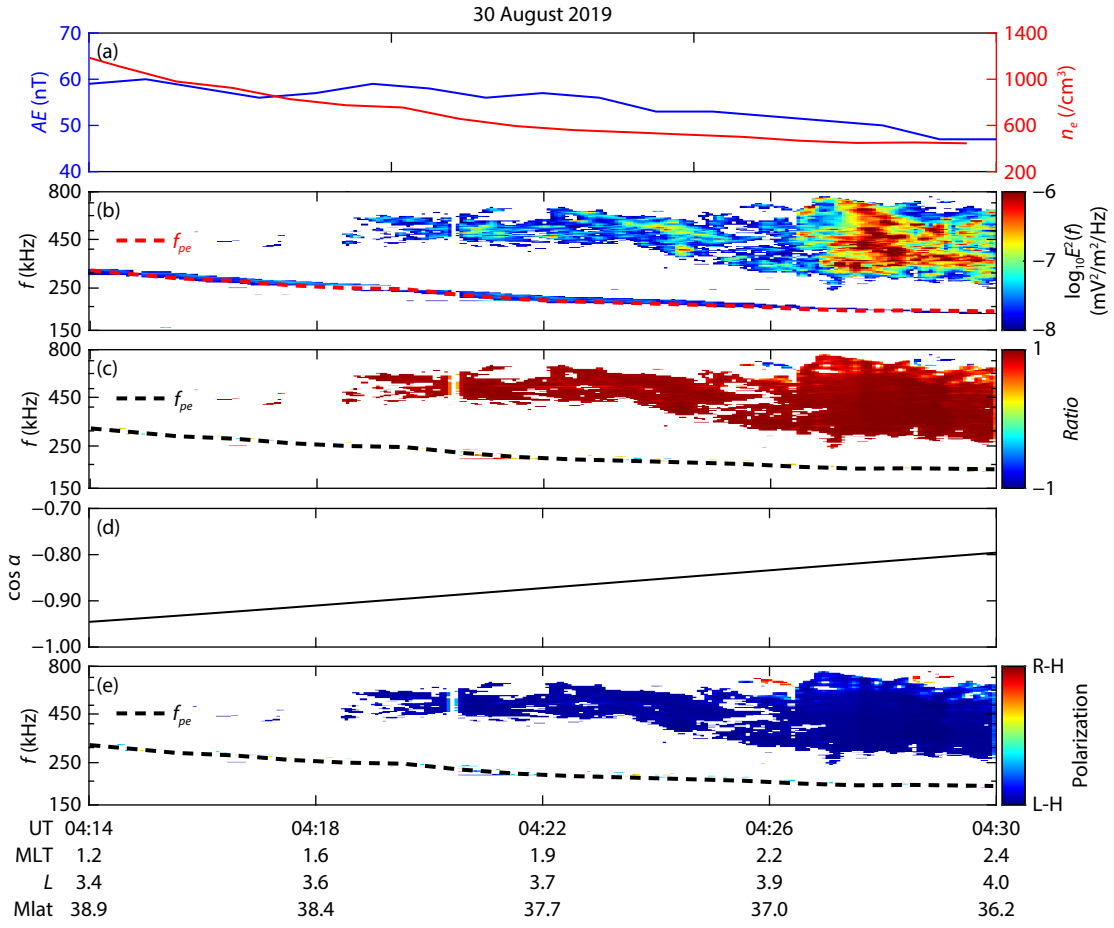

Figure 3. Nightside L-O mode AKR (Event C) observed by the Arase satellite during 04:14–04:30 UT on 30 August 2019. (a) The *AE* index (blue line) and plasma density (red line). (b) The electric field spectra measured by the HFA (the red dashed line corresponds to the f_{pe}). (c) The raw *Ratio* of emissions with PSD $\geq 10^{-8}$ mV^{2}m^{-2}Hz^{-1} (the black dashed line represents the f_{pe}). (d) The cosine α. (e) The polarization of emissions with PSD $\geq 10^{-8}$ mV^{2}m^{-2}Hz^{-1} (the black dashed line corresponds to the f_{pe}).

Figure 3a). Figure 3c shows the *Ratio* from the Arase satellite observation. Figure 3d plots the cosine α. The polarization (Figure 3e) shows positive *Ratio* values (Figure 3c), as the spin axis is against the background field direction on the nightside of the northern hemisphere (Figure 3d). This identifies the significant AKR emission above f_{pe} as L-O mode. Figure 4 shows the example of L-O mode emission (Event D), with frequency ranging from 100 to 400 kHz, occurred on the dayside (MLT = 12.7–13.9), which is observed at 13:20–14:40 UT when the geomagnetic condition is disturbed (*AE* index was between 150–250 nT). The polarization (Figure 4e) shows negative *Ratio* values (Figure 4c), as the spin axis is parallel the background field direction on the dayside of the northern hemisphere (Figure 4d). This identifies the significant AKR emission above f_{pe} as L-O mode as well. This event confirms that the PSD of L-O mode AKR on dayside can approach 10^{-7} mV^{2}m^{-2}Hz^{-1}.

Examples of L-X mode AKR emission are presented in Figures 5–6. Figure 5 captures intense nightside AKR emission (Event E) spanning MLT = 22.0–23.9, Mlat = 35.4°–36.2° recorded between 07:15 to 07:35 UT on 14 January 2019. During this interval, geomagnetic activity remained low, as indicated by the *AE* index (blue line, Figure 5a), which fluctuated mildly between 30 and 60 nT, which a rise in plasma density to 1200 cm^{-3} (red line). The black solid line and black dashed line in Figures 5c and 5e represent f_{pe} and f_{LX}, respectively. The AKR emissions exhibited clear L-X mode characteristics, evidenced by a positive *Ratio* value (Figure 5c) and the spin axis against the background magnetic field (Figure 5d). In contrast, Figure 6 illustrates the dayside (MLT = 12.9–13.8) L-X mode emission (Event F) detected at 21:45–22:25 UT on 23 January 2019 during a enhanced geomagnetic activity with *AE* could reach ~300 nT. The emissions, staying between f_{pe} and f_{LX}, covered a relatively narrow frequency range (20–30 kHz). The negative *Ratio* values (Figure 6c) for these emission and the spin axis aligned with the background magnetic field (Figure 6d) demonstrates that dayside L-X mode AKR can attain PSD levels comparable to nightside with the maximum value 10^{-6} mV^{2}m^{-2}Hz^{-1}.

4. Summary

Auroral kilometric radiation (AKR) is an important intense electromagnetic emission in the magnetosphere characterized by wavelengths on the order of kilometers. Previous studies have shown that the majority of AKR stay in the right-handed extraordinary (R-X) mode, with a small observation in the left-handed ordinary (L-O) and left-handed extraordinary (L-X) modes. While the contri-

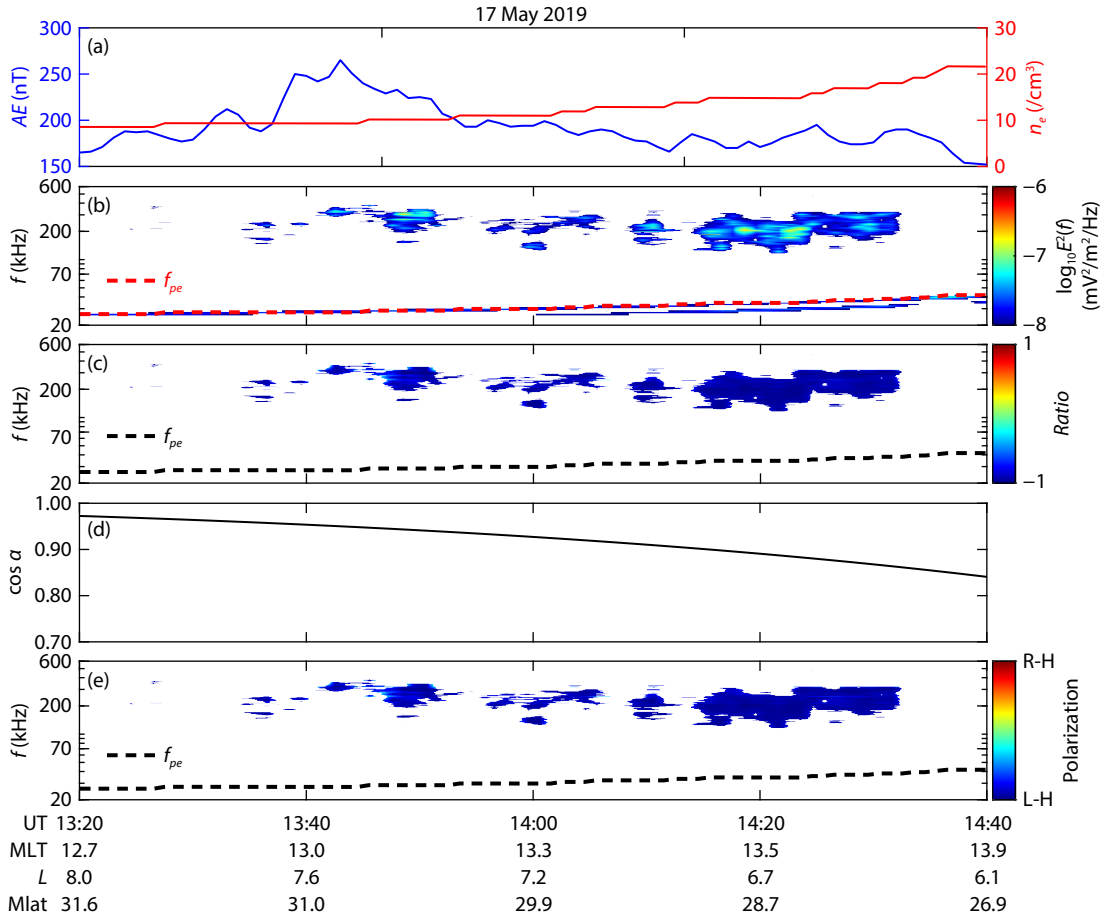

Figure 4. Dayside L-O mode AKR (Event D) observed by the Arase satellite during 13:20–14:40 UT on 17 May 2019. Same format as Figure 3.

bution of AKR to the magnetosphere–ionosphere–atmosphere coupling is sensitively to the mode. Here, we comprehensively introduce the practical polarization analysis method for the high frequency observations of Arase satellite. The sign of the *Ratio* corresponds to the polarization: under the condition that the satellite spin axis is parallel to the background magnetic field (***B***), the positive (negative) *Ratio* presents the right-handed (left-handed) polarization. In contrast, when the spin axis is anti-parallel to ***B***, the correspondence between the polarization and ratio sign is reversed. According to the polarization data and frequency ranges, two events of each mode of AKR are systematically reported for the first time. Observations show that three modes can be observed both on the dayside and nightside, and the intensity of three modes can reach 10^{-6} mV^{2}m^{-2}Hz^{-1}. This study enriches our understanding of AKR in the Earth's magnetosphere and similar emission in other planet.

Open Research Section

Science data of the ERG (Arase) satellite was obtained from the ERG Science Center operated by ISAS/JAXA and ISEE/Nagoya University (https://ergsc.isee.nagoya-u.ac.jp/data/ergsc/satellite/erg/, Miyoshi, Hori et al., 2018). The present study analyzed PWE-HFA-L2 v01_02 data (doi:10.34515/DATA.ERG-10000) and Orbit-L2 v02 data (10.34515/DATA.ERG-1 2000). The *AE* index data was downloaded from http://wdc.kugi.kyoto-u.ac.jp/aeasy/index.html.

Acknowledgments

This work is supported by the National Natural Science Foundation of China (Grants 42374215, 42230209, 42374199, 42304183, 42422406, 42174185, 72061147004 and 72342001), the Science and Technology Development Fund, Macau SAR (File no. 0042/2024/RIA1 and 0008/2024/AKP), the Natural Science Foundation of Hunan Province (Grant 2023JJ20038), the Research Project of Science and Technology of Hunan Province (2025JJ10009, 2022RC4025, 2025QK1004, 2023JJ50312, 2023JJ50010 and 2024RC9012).

References

Baker, D. N. (2002). How to cope with space weather. *Science*, *297*(5586), 1486–1487. https://doi.org/10.1126/science.1074956

Benson, R. F. (1985). Auroral kilometric radiation: Wave modes, harmonics, and source region electron density structures. *J. Geophys. Res.: Space Phys.*, *90*(A3), 2753–2784. https://doi.org/10.1029/JA090iA03p02753

Benson, R. F., Mellott, M. M., Huff, R. L., and Gurnett, D. A. (1988). Ordinary mode auroral kilometric radiation fine structure observed by DE 1. *J. Geophys. Res.: Space Phys.*, *93*(A7), 7515–7520. https://doi.org/10.1029/JA093iA07p07515

Burinskaya, T. M. (2013). Ray tracing model of the auroral kilometric radiation generation in the 3-D plasma cavity. *Ann. Geophys.*, *31*(10), 1645–1652. https://doi.org/10.5194/angeo-31-1645-2013

Callis, L. B., Natarajan, M., Evans, D. S., and Lambeth, J. D. (1998). Solar atmospheric coupling by electrons (SOLACE): 1. Effects of the May 12, 1997 solar event on the middle atmosphere. *J. Geophys. Res.: Atmos.*, *103*(D21), 28405–28419. https://doi.org/10.1029/98JD02408

Calvert, W. (1981a). The auroral plasma cavity. *Geophys. Res. Lett.*, *8*(8), 919–921.

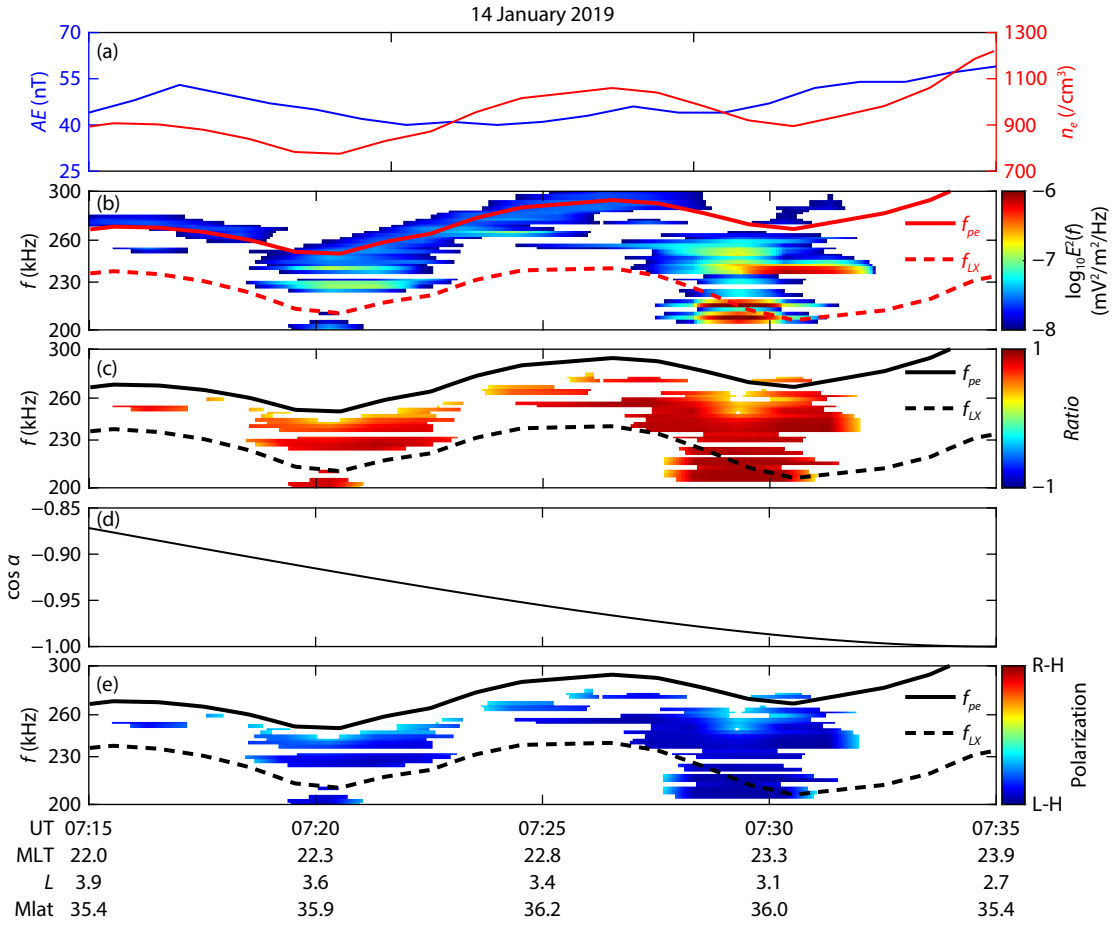

Figure 5. Nightside L-X mode AKR (Event E) observed by the Arase satellite during 07:15–07:35 UT on 14 January 2019. (a) The *AE* index (blue line) and plasma density (red line). (b) The electric field spectra measured by the HFA (the red solid line denotes the f_{pe} and the red dashed line is the f_{LX}). (c) The raw *Ratio* of emissions with PSD $\geq 10^{-8}$ mV^{2}m^{-2}Hz^{-1} (the black solid line denotes the f_{pe} and the black dashed line is the f_{LX}). (d) The cosine α. (e) The polarization of emissions with PSD $\geq 10^{-8}$ mV^{2}m^{-2}Hz^{-1} (the black solid line denotes the f_{pe} and the black dashed line is the f_{LX}).

https://doi.org/10.1029/GL008i008p00919

Calvert, W. (1981b). The signature of auroral kilometric radiation on Isis 1 ionograms. *J. Geophys. Res.: Space Phys.*, *86*(A1), 76–82. https://doi.org/10.1029/JA086iA01p00076

Calvert, W. (1995). An explanation for auroral structure and the triggering of auroral kilometric radiation. *J. Geophys. Res.: Space Phys.*, *100*(A8), 14887–14894. https://doi.org/10.1029/95JA00523

Delory, G. T., Ergun, R. E., Carlson, C. W., Muschietti, L., Chaston, C. C., Peria, W., McFadden, J. P., and Strangeway, R. (1998). FAST observations of electron distributions within AKR source regions. *Geophys. Res. Lett.*, *25*(12), 2069–2072. https://doi.org/10.1029/98GL00705

Deng, Z. K., Xiao, F. L., Zhou, Q. H., Zhang, S., Liu, S., Yang, Q. W., Tang, J. W., Kumamoto, A., Miyoshi, Y., … Nakamura, S. (2022). Direct evidence for auroral kilometric radiation propagation into radiation belts based on Arase spacecraft and Van Allen Probe B. *Geophys. Res. Lett.*, *49*(19), e2022GL100860. https://doi.org/10.1029/2022GL100860

Ergun, R. E., Carlson, C. W., Mcfadden, J. P., Mozer, F. S., Delory, G. T., Peria, W., Chaston, C. C., Temerin, M., Elphic, R., … Kistler, L. (1998). FAST satellite wave observations in the AKR source region. *Geophys. Res. Lett.*, *25*(12), 2061–2064. https://doi.org/10.1029/98GL00570

Green, J. L., Boardsen, S., Garcia, L., Fung, S. F., and Reinisch, B. W. (2004). Seasonal and solar cycle dynamics of the auroral kilometric radiation source region. *J. Geophys. Res.: Space Phys.*, *109*(A5), 2003JA010311. https://doi.org/10.1029/2003JA010311

Gurnett, D. A., Shawhan, S. D., and Shaw, R. R. (1983). Auroral hiss, *Z* mode radiation, and auroral kilometric radiation in the polar magnetosphere: DE 1 observations. *J. Geophys. Res.: Space Phys.*, *88*(A1), 329–340. https://doi.org/10.1029/JA088iA01p00329

Hanasz, J., Boudjada, M. Y., Schreiber, R., Krawczyk, Z., Malycha, M., Mogilevsky, M. M., Rucker, H. O., and Romantsova, T. V. (2000). Dynamic spectra of the Stokes parameters for the dayside and nightside auroral kilometric radiation. *Geophys. Res. Lett.*, *27*(11), 1631–1634. https://doi.org/10.1029/1999GL010770

Hanasz, J., Panchenko, M., De Feraudy, H., Schreiber, R., and Mogilevsky, M. M. (2003). Occurrence distributions of the auroral kilometric radiation ordinary and extraordinary wave modes. *J. Geophys. Res.: Space Phys.*, *108*(A11), 2002JA009579. https://doi.org/10.1029/2002JA009579

Jiao, L. H., Ma, X., Zhang, Y. N., Jin, T. F., Fu, S., and Ni, B. B. (2024). A statistical analysis of the Kappa-type energy spectrum distribution of radiation belt electrons observed by Van Allen Probes. *Earth Planet. Phys.*, *8*(2), 368–375. https://doi.org/10.26464/epp2024001

Jin, T. F., Ni, B. B., Fu, S., Yun, X. T., Pang, S. Y., Long, M. Y., Zhang, Q. Y., Wang, N., Xiong, X. J., Zhao, Y. B., and Shi, F. F. (2025). Modulation of suprathermal electron fluxes by ultra-low-frequency magnetic field fluctuations in the Martian foreshock. *Earth Planet. Phys.*, *9*(2), 357–365. https://doi.org/10.26464/epp2025027

Kaiser, M. L., Alexander, J. K., Riddle, A. C., Pearce, J. B., and Warwick, J. W. (1978). Direct measurements by Voyagers 1 and 2 of the polarization of terrestrial kilometric radiation. *Geophys. Res. Lett.*, *5*(10), 857–860. https://doi.org/10.1029/GL005i010p00857

Kasaba, Y., Ishisaka, K., Kasahara, Y., Imachi, T., Yagitani, S., Kojima, H., Matsuda, S., Shoji, M., Kurita, S., … Nomura, R. (2017). Wire Probe Antenna (WPT) and

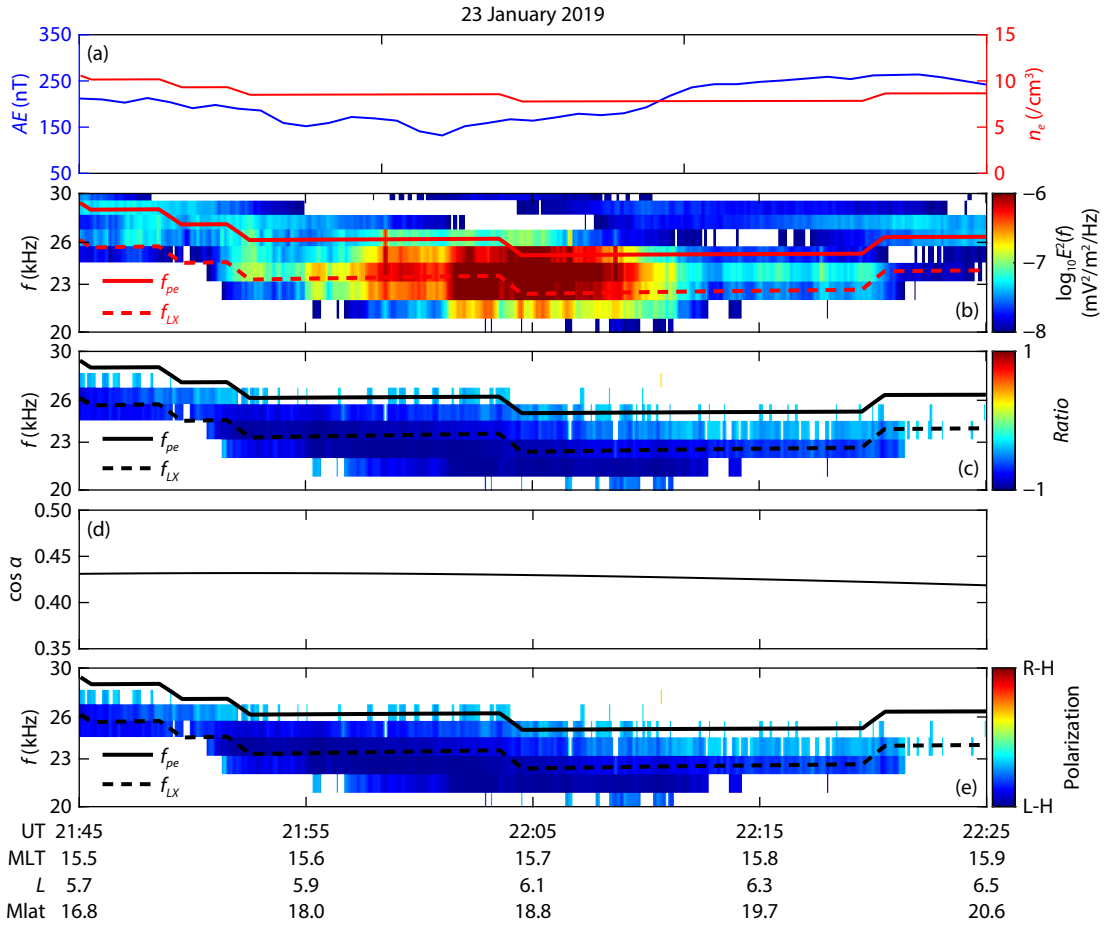

Figure 6. Dayside L-X mode AKR (Event F) observed by the Arase satellite during 21:45–22:25 UT on 23 January 2019. Same format as Figure 5.

Electric Field Detector (EFD) of Plasma Wave Experiment (PWE) aboard the Arase satellite: specifications and initial evaluation results. *Earth, Planets Space*, *69*(1), 174. https://doi.org/10.1186/s40623-017-0760-x

Kasahara, Y., Kasaba, Y., Kojima, H., Yagitani, S., Ishisaka, K., Kumamoto, A., Tsuchiya, F., Ozaki, M., Matsuda, S., … Shinohara, I. (2018). The Plasma Wave Experiment (PWE) on board the Arase (ERG) satellite. *Earth, Planets Space*, *70*(1), 86. https://doi.org/10.1186/s40623-018-0842-4

Kumamoto, A., Ono, T., Iizima, M., and Oya, H. (2003). Seasonal and solar cycle variations of the vertical distribution of the occurrence probability of auroral kilometric radiation sources and of upflowing ion events. *J. Geophys. Res.: Space Phys.*, *108*(A1), 1032. https://doi.org/10.1029/2002JA009522

Kumamoto, A., Tsuchiya, F., Kasahara, Y., Kasaba, Y., Kojima, H., Yagitani, S., Ishisaka, K., Imachi, T., Ozaki, M., … Obara, T. (2018). High Frequency Analyzer (HFA) of Plasma Wave Experiment (PWE) onboard the Arase spacecraft. *Earth, Planets Space*, *70*(1), 82. https://doi.org/10.1186/s40623-018-0854-0

Kurth, W. S., Baumback, M. M., and Gurnett, D. A. (1975). Direction-finding measurements of auroral kilometric radiation. *J. Geophys. Res.*, *80*(19), 2764–2770. https://doi.org/10.1029/JA080i019p02764

Kurth, W. S., and Gurnett, D. A. (1998). Auroral kilometric radiation integrated power flux as a proxy for A_E. *Adv. Space Res.*, *22*(1), 73–77. https://doi.org/10.1016/S0273-1177(97)01103-4

Li, P., Zhang, S., Xiao, F. L., Yang, H. M., Ye, S. Y., Liu, S., He, Y. H., Yang, Q. W., Tang, J. W., and Johnston, A. J. (2024). Annual and seasonal occurrence pattern of auroral kilometric radiation associated with the interplanetary magnetic field. *Astrophys. J. Lett.*, *966*(2), L26. https://doi.org/10.3847/2041-8213/ad40a7

Liou, K., Meng, C. I., Lui, A. T. Y., Newell, P. T., and Anderson, R. R. (2000). Auroral kilometric radiation at substorm onset. *J. Geophys. Res.: Space Phys.*, *105*(A11), 25325–25331. https://doi.org/10.1029/2000JA000038

Mellott, M. M., Calvert, W., Huff, R. L., Gurnett, D. A., and Shawhan, S. D. (1984). DE-1 observations of ordinary mode and extraordinary mode auroral kilometric radiation. *Geophys. Res. Lett.*, *11*(12), 1188–1191. https://doi.org/10.1029/GL011i012p01188

Melrose, D. B., Rönnmark, K. G., and Hewitt, R. G. (1982). Terrestrial kilometric radiation: The cyclotron theory. *J. Geophys. Res.: Space Phys.*, *87*(A7), 5140–5150. https://doi.org/10.1029/JA087iA07p05140

Miyoshi, Y., Shinohara, I., Takashima, T., Asamura, K., Higashio, N., Mitani, T., Kasahara, S., Yokota, S., Kazama, Y., … Seki, K. (2018). Geospace exploration project ERG. *Earth, Planets Space*, *70*(1), 101. https://doi.org/10.1186/s40623-018-0862-0

Mogilevsky, M. M., Moiseenko, I. L., and Hanasz, J. (2005). Spectral variations and long-period intensity variations of auroral kilometric radiation from INTERBALL-2 satellite measurements. *Astron. Lett.*, *31*(6), 422–426. https://doi.org/10.1134/1.1940115

Mutel, R. L., Peterson, W. M., Jaeger, T. R., and Scudder, J. D. (2007). Dependence of cyclotron maser instability growth rates on electron velocity distributions and perturbation by solitary waves. *J. Geophys. Res.: Space Phys.*, *112*(A7), A07211. https://doi.org/10.1029/2007JA012442

Mutel, R. L., Christopher, I. W., and Pickett, J. S. (2008). Cluster multispacecraft determination of AKR angular beaming. *Geophys. Res. Lett.*, *35*(7), L07104. https://doi.org/10.1029/2008GL033377

Nakamura, Y., Fukuda, S., Shibano, Y., Ogawa, H., Sakai, S. I., Shimizu, S., Soken, E., Miyazawa, Y., Toyota, H., … Shinohara, I. (2018). Exploration of energization and radiation in geospace (ERG): challenges, development, and operation of satellite systems. *Earth, Planets Space*, *70*(1), 102. https://doi.org/10.1186/s40623-018-0863-z

Oya, H., and Morioka, A. (1983). Observational evidence of *Z* and *L-O* mode waves as the origin of auroral kilometric radiation from the Jikiken (EXOS-B) satellite. *J. Geophys. Res.: Space Phys.*, *88*(A8), 6189–6203. https://doi.org/10.1029/JA088iA08p06189

Panchenko, M. (2004). Polarimetry of auroral kilometric radiation with a triaxial nonorthogonal antenna system. *Radio Sci.*, *39*(6), RS6010. https://doi.org/10.1029/2004RS003039

Pritchett, P. L. (1984). Relativistic dispersion, the cyclotron maser instability, and auroral kilometric radiation. *J. Geophys. Res.: Space Phys.*, *89*(A10), 8957–8970. https://doi.org/10.1029/JA089iA10p08957

Pritchett, P. L., Strangeway, R. J., Ergun, R. E., and Carlson, C. W. (2002). Generation and propagation of cyclotron maser emissions in the finite auroral kilometric radiation source cavity. *J. Geophys. Res.: Space Phys.*, *107*(A12), 1437. https://doi.org/10.1029/2002JA009403

Schreiber, R., Panchenko, M., Hanasz, J., Mutel, R., and Christopher, I. (2017). Beaming of intense AKR seen from the Interball-2 spacecraft. *J. Geophys. Res.: Space Phys.*, *122*(1), 249–257. https://doi.org/10.1002/2015JA022197

Seki, T., Morioka, A., Miyoshi, Y. S., Tsuchiya, F., Misawa, H., Gonzalez, W., Sakanoi, T., Oya, H., Matsumoto, H., … Mukai, T. (2005). Auroral kilometric radiation and magnetosphere-ionosphere coupling process during magnetic storms. *J. Geophys. Res.: Space Phys.*, *110*(A5), A05206. https://doi.org/10.1029/2004JA010961

Shawhan, S. D., and Gurnett, D. A. (1982). Polarization measurements of auroral kilometric radiation by Dynamics Explorer-1. *Geophys. Res. Lett.*, *9*(9), 913–916. https://doi.org/10.1029/GL009i009p00913

Sonwalkar, V. S., Carpenter, D. L., Bell, T. F., Spasojević, M., Inan, U. S., Li, J., Chen, X., Venkatasubramanian, A., Harikumar, J., … Reinisch, B. W. (2004). Diagnostics of magnetospheric electron density and irregularities at altitudes <5000 km using whistler and Z mode echoes from radio sounding on the IMAGE satellite. *J. Geophys. Res.: Space Phys.*, *109*(A11), A11212. https://doi.org/10.1029/2004JA010471

Summers, D., Thorne, R. M., and Xiao, F. L. (2001). Gyroresonant acceleration of electrons in the magnetosphere by superluminous electromagnetic waves. *J. Geophys. Res.: Space Phys.*, *106*(A6), 10853–10868. https://doi.org/10.1029/2000JA000309

Tang, J. W., Zhang, S., Xiao, F. L., Yang, H. M., Liu, S., He, Y. H., Yang, C., Jin, Y. Y., Deng, Z. K., … James Johnston, A. (2025). Distinct MLT asymmetry of auroral kilometric radiation observed by the FAST satellite. *Earth Planet. Phys.*, *9*(1), 188–193. https://doi.org/10.26464/epp2024079

Thorne, R. M. (1977). Energetic radiation belt electron precipitation: A natural depletion mechanism for stratospheric ozone. *Science*, *195*(4275), 287–289. https://doi.org/10.1126/science.195.4275.287

Thorne, R. M., O'Brien, T. P., Shprits, Y. Y., Summers, D., and Horne, R. B. (2005). Timescale for MeV electron microburst loss during geomagnetic storms. *J. Geophys. Res.: Space Phys.*, *110*(A9), A09202. https://doi.org/10.1029/2004JA010882

Wu, C. S., and Lee, L. C. (1979). A theory of the terrestrial kilometric radiation. *Astrophys. J.*, *230*, 621–626. https://doi.org/10.1086/157120

Xiao, F. L., He, H. Y., Zhou, Q. H., Zheng, H. N., and Wang, S. (2006). Relativistic diffusion coefficients for superluminous (auroral kilometric radiation) wave modes in space plasmas. *J. Geophys. Res.: Space Phys.*, *111*(A11), A11201. https://doi.org/10.1029/2006JA011865

Xiao, F. L., Su, Z. P., Chen, L. X., Zheng, H. N., and Wang, S. (2010). A parametric study on outer radiation belt electron evolution by superluminous R-X mode waves. *J. Geophys. Res.: Space Phys.*, *115*(A10), A10217. https://doi.org/10.1029/2010JA015374

Xiao, F. L., Chen, L. X., and He, Y. H. (2011). Bounce-averaged diffusion coefficients for superluminous wave modes in the magnetosphere. *J. Atmos. Sol.-Terr. Phys.*, *73*(1), 88–94. https://doi.org/10.1016/j.jastp.2009.12.012

Xiao, F. L., Zhou, Q. H., Su, Z. P., He, Z. G., Yang, C., Liu, S., He, Y. H., and Gao, Z. L. (2016). Explaining occurrences of auroral kilometric radiation in Van Allen radiation belts. *Geophys. Res. Lett.*, *43*(23), 11971–11978. https://doi.org/10.1002/2016GL071728

Xiao, F. L., Tang, J. W., Zhang, S., Zhou, Q. H., Liu, S., He, Y. H., Yang, Q. W., Kasahara, Y., Miyoshi, Y., … Nakamura, S. (2022). Asymmetric distributions of auroral kilometric radiation in Earth's northern and southern hemispheres observed by the Arase satellite. *Geophys. Res. Lett.*, *49*(13), e2022GL099571. https://doi.org/10.1029/2022GL099571

Zarka, P. (1998). Auroral radio emissions at the outer planets: Observations and theories. *J. Geophys. Res.: Planets*, *103*(E9), 20159–20194. https://doi.org/10.1029/98JE01323

Zhang, S., Shang, X. J., He, Y. H., Liu, S., and Xiao, F. L. (2020). Dominant roles of high harmonics on interactions between AKR and radiation belt relativistic electrons. *Geophys. Res. Lett.*, *47*(16), e2020GL088421. https://doi.org/10.1029/2020GL088421

Zhang, S., Liu, S., Li, W. T., He, Y. H., Yang, Q. W., Xiao, F. L., Kumamoto, A., Miyoshi, Y., Nakamura, Y., … Shinohara, I. (2021). A concise empirical formula for the field-aligned distribution of auroral kilometeric radiation based on Arase satellite and Van Allen Probes. *Geophys. Res. Lett.*, *48*(8), e2021GL092805. https://doi.org/10.1029/2021GL092805

Zhang, S., Yin, Q. P., Yang, H. M., Xiao, F. L., Zhou, Q. H., Yang, Q. W., Tang, J. W., Deng, Z. K., Kasahara, Y., … Hori, T. (2024). Direct observation of L-X mode of auroral kilometric radiation in the lower latitude magnetosphere by the Arase satellite. *Geophys. Res. Lett.*, *51*(5), e2023GL105694. https://doi.org/10.1029/2023GL105694

Zhao, W. L., Liu, S., Zhang, S., Zhou, Q. H., Yang, C., He, Y. H., Gao, Z. L., and Xiao, F. L. (2019). Global occurrences of auroral kilometric radiation related to suprathermal electrons in radiation belts. *Geophys. Res. Lett.*, *46*(13), 7230–7236. https://doi.org/10.1029/2019GL083944